Neuropharmacology 179 (2020) 108265

Contents lists available at ScienceDirect

Neuropharmacology

journal homepage: www.elsevier.com/locate/neuropharm

Invited review

Computational studies on cholinesterases: Strengthening our understanding of the integration of structure, dynamics and function

Joel L. Sussman [a,*], Israel Silman [b]

[a] Department of Structural Biology, Weizmann Institute of Science, Rehovot, Israel
[b] Department of Neurobiology, Weizmann Institute of Science, Rehovot, Israel

ARTICLE INFO

Keywords:
Acetylcholinesterase
Butyrylcholinesterase
PROSS
Docking
Molecular dynamics
Structure reassessment

ABSTRACT

Computational approaches have proved valuable in elucidating structure/function relationships in the cholinesterases in the context of their unusual three-dimensional structure. In this review we survey several recent studies that have enhanced our understanding of how these enzymes function, and have utilized computational approaches both to modulate their activity and to improve the design of lead compounds for their inhibition. An animated Interactive 3D Complement (I3DC) is available in Proteopedia at http://proteopedia.org/w/Journal:Neuropharmacology:2

1. Introduction

Solution of the crystal structure of *Torpedo californica* acetylcholinesterase (*Tc*AChE) in 1991 (Sussman et al., 1991), revealed a three-dimensional structure that was wholly unanticipated. Despite the fact that AChE is one of the most rapid enzymes known, operating at a speed approaching diffusion control (Bazelyansky et al., 1986; Rosenberry, 1975), its active site is deeply buried, at the bottom of a long and narrow gorge, whose cross-section, at its narrowest point, is significantly smaller than the cross-section of the quaternary group of acetylcholine (ACh). Subsequent solution of the crystal structures of mouse (m) (Bourne et al., 1995), *Electrophorus electricus* (*Ee*) (Bourne et al., 1999; Raves et al., 1998), human (h) (Cheung et al., 2012; Kryger et al., 2000), *Drosophila melanogaster* (*Dm*) (Harel et al., 2000), *Bungarus fasciatus* (*Bf*) (Bourne et al., 2015), and *Anopheles gambiae* (*Ag*) (Cheung et al., 2018; Han et al., 2018) AChEs, as well as that of human serum butyrylcholinesterase (hBChE) (Nicolet et al., 2003), revealed highly homologous structures. The crystal structures of the cholinesterases (ChEs) raised cogent questions with respect to the coupling of the structure of the enzymes, together with their dynamics, to their catalytic activity, and to the way in which inhibitors, some of which are large and rigid, bind to, and disassociate from them. These topics have been covered extensively in earlier reviews (Silman and Sussman, 2008; Xu et al., 2017). However, as computing power has continued to grow, databases have expanded, and increasingly sophisticated algorithms have been developed, problems become accessible that had previously seemed unapproachable (Fuxreiter, 2015). In the following, after briefly surveying the structure and dynamics of the ChEs, taking *Tc*AChE as the prototypic case, we wish to briefly present and discuss some recent studies that cover various aspects of these topics.

2. Overall structure and dynamics

As stated above, we will use *Tc*AChE as the prototypic template, and only refer to other structures where there are relevant differences of structural and functional significance.

As already mentioned, solution of the crystal structure of *Tc*AChE revealed that despite its high catalytic turnover rate for its natural substrate, ACh, its active-site is buried near the bottom of a deep and narrow cavity, >15 Å deep (Sussman et al., 1991). This cavity has been named the active-site gorge, or the aromatic gorge, since it is lined by 14 conserved aromatic residues, the rings of which account for ~70% of its surface, to many of which functional/structural roles can be assigned. Two functional binding sites can be distinguished - a catalytic 'anionic' site (CAS), adjacent to the catalytic triad, near the bottom of the gorge, and a peripheral 'anionic' site (PAS), near the top of the gorge. The latter serves as an initial binding site for ACh, and powerful bi-functional inhibitors have been designed, whose potency arises from the fact that they are elongated ligands that span the CAS and the PAS (Harel et al., 1993). Although these sites are called 'anionic' they do not contain anionic groups (*e.g.*, carboxylates), but rather conserved aromatic residues, the aromatic rings of which make π-cation interactions with the

* Corresponding author.
E-mail address: Joel.Sussman@weizmann.ac.il (J.L. Sussman).

https://doi.org/10.1016/j.neuropharm.2020.108265
Received 3 April 2020; Received in revised form 21 May 2020; Accepted 27 July 2020
Available online 11 August 2020

quaternary group of ACh, the principal residues involved being W84 in the CAS, and W279 in the PAS (*Tc*AChE numbering, and also below, unless stated otherwise). Accordingly, a constructive suggestion has been made that the two sites be renamed as the catalytic aromatic site and the peripheral aromatic site, respectively. If this change in nomenclature were to be adopted, the abbreviations, CAS and PAS, would be 'conserved'.

Closer inspection of the crystal structure revealed two features shared by the AChEs:

- A bottleneck, about halfway down the gorge, formed by two aromatic residues, F330 and Y121. The cross-section of the gorge at the bottleneck is smaller than the diameter of the quaternary group of ACh, implying that the enzyme must breathe substantially for the substrate to reach the active site (Colletier et al., 2006).
- An asymmetric charge distribution, resulting in an enormous dipole moment of ~1000 Debye (Porschke et al., 1996; Ripoll et al., 1993). The dipole moment is oriented approximately along the axis of the active-site gorge, and its direction is such that the positively charged ACh is attracted towards the active site (Botti et al., 1999; Felder et al., 1997).

The fact that the ACh is driven towards the active site by a strong electric field raised the question of how the choline moiety produced by substrate hydrolysis would exit the gorge. It was suggested that rather than exiting back along the gorge it might to do so via a 'back door', near the active site at the bottom of the gorge (Ripoll et al., 1993). Indeed, MD simulations suggested a candidate exit route (Gilson et al., 1994). Subsequently, when greatly increased computing power had become available, the issue was revisited, and the back door was more accurately identified by use of MD (Xu et al., 2010). Furthermore, it was shown to correspond exactly to a back door that was identified by X-ray crystallography (Sanson et al., 2011), which was located at the seam between the two sub-domains of which the enzyme is composed (Morel et al., 1999). hBChE has a high dipole moment similar to that of the AChEs (Felder et al., 1997). Moreover, the three aromatic residues at the backdoor of *Tc*AChE, *viz.*, W84, W432, and Y442, are conserved in hBChE (Harel et al., 1992). Thus, the back-door exit appears to be similarly conserved (Silman & Sussman, unpublished).

As to the structural basis for the high catalytic activity displayed by AChE, the crystal structure of the complex of *Tc*AChE with a powerful transition state analog revealed that it was completely enveloped by the enzyme, making multiple interactions that generate a highly favorable transition state (Harel et al., 1996), and the substrate, acetylthiocholine, is similarly enveloped (Colletier et al., 2006). Similar structural data have also been obtained for mAChE (Bourne et al., 2006).

The above description of structure/function relationships in *Tc*AChE adequately describes the similar relationships in other vertebrate AChEs that have been studied, with only minor differences in structure being observed. The insect AChEs, *Ag*AChE and *Dm*AChE, differ somewhat more, but not in any fundamental features (Cheung et al., 2018; Harel et al., 2000; Nachon et al., 2020). The same cannot be said, however, for BChE. The human enzyme (hBChE) displays high sequence homology (53%) to *Tc*AChE, with no additions or deletions in their first 535 residues, and possesses the same three intrachain disulfides (Harel et al., 1992). However, its active-site gorge is very different from that of AChE. Six of the 14 conserved aromatic residues present in *Tc*AChE are lacking in hBChE. Although the key Trp residue with which ACh interacts at the CAS is retained, W84 in *Tc*AChE, W82 in hBChE - the residues homologous to the two residues in the bottleneck, Y121 and F330, and to the two aromatic residues in the PAS, W279 and Y70, are all replaced by non-aromatic, and consequently much smaller, residues. Thus, the active-site gorge of hBChE is less complex, and much more open, than that of *Tc*AChE (Nicolet et al., 2003). It also lacks the aromatic residues of the PAS. However, it displays an alternative PAS whose principal member is Y70 (Masson et al., 1996). Although it is rather difficult to directly compare their catalytic efficacies, since AChE displays substrate inhibition (Colletier et al., 2006), whereas BChE displays substrate activation (Masson et al., 1996), BChE also displays very high catalytic activity on ACh. Nevertheless, the maximal activity values reported for AChE are several-fold higher than those for BChE (Mukhametgalieva et al., 2019). Thus, the more complex structure of AChE may be a requirement for it to achieve the catalytic power necessary for rapid termination of impulse transmission at cholinergic synapses.

π-Cation interactions are important structural motifs in the ChEs (Harel et al., 1993), as well as in both nicotinic and muscarinic receptors. Indeed, the ACh-binding site in these receptors has been called the 'aromatic cage' (Hulme et al., 2003; Post et al., 2017). Furthermore, π-cation and π-π stacking interactions are involved in the binding of many ligands to the ChEs. Several of the commonly employed docking programs, such as Autodock (Goodsell et al., 1996) and GOLD (Jones et al., 1995, 1997) do not take into account either of these types of interaction, and thus are most unsuitable choices when AChE or BChE are the docking targets. A case in point is the docking of methylene blue to AChE, where Autodock and Autodock vina both performed poorly (Wildman et al., 2011). In order to achieve a result that matched the experimental data it was found necessary to use Glide XP within the Schrodinger software suite (Halgren et al., 2004; Friesner et al., 2004, 2006).

Another issue with general implications, but which applies especially to the active-site gorge in the ChEs, is the presence of conserved waters in the active-site gorge (Koellner et al., 2000). Some of these waters are tightly bound to amino acid residues lining the gorge, and may effectively considered as part of the protein template with which a ligand interacts. However, not only conserved waters may be present in a protein structure, but also solvent molecules that serve as precipitants in the crystallization conditions. They, too, may occupy sites that may need to be considered as part of the protein template when docking protocols are implemented. A large proportion of the crystal structures deposited in the PDB were obtained for crystals obtained using PEGs as precipitants. But, as we have pointed out (Dym et al., 2016), in most structures no PEGs are assigned. We will return to this important issue in Part 7.

3. The PROSS algorithm permits large-scale expression of AChE and BChE in a prokaryotic expression system

Expression of a eukaryotic protein in a prokaryotic expression system usually permits its production in much larger amounts, and at a much lower cost, than in a eukaryotic expression system (Zemella et al., 2015). Expression of both AChE and BChE in a prokaryotic host is an important objective because both civilian and military organizations have been interested in their large-scale utilization as both prophylactic and therapeutic bioscavengers for treatment of intoxication by organophosphate (OP) nerve agents and insecticides (Lushchekina et al., 2018), and as decontaminants of the same OP compounds, whether in the context of elimination of environmental pollution or for decontamination of equipment or personnel (Maxwell et al., 1999).

Many unsuccessful attempts to express the ChEs in prokaryotic expression systems were made over several decades - mostly unpublished. In an early attempt, hAChE was expressed as inclusion bodies in *E. coli*, and very small amounts of active enzyme were obtained by solubilization of the inclusion bodies under denaturing conditions followed by renaturation (Fischer et al., 1995), and expression of rat AChE was similarly unsuccessful (Heim et al., 1998; Masson et al., 1992).

A novel algorithm was developed, PROSS, which stands for Protein Repair One Stop Shop - http://pross.weizmann.ac.il. It was designed to predict amino acid substitutions that would improve the expression and stability of proteins (Goldenzweig et al., 2016). To this end it scans the entire protein sequence, using bioinformatics sequence alignment tools, and introduces mutations that are predicted to improve such characteristics as core packing, surface polarity and backbone rigidity, at the

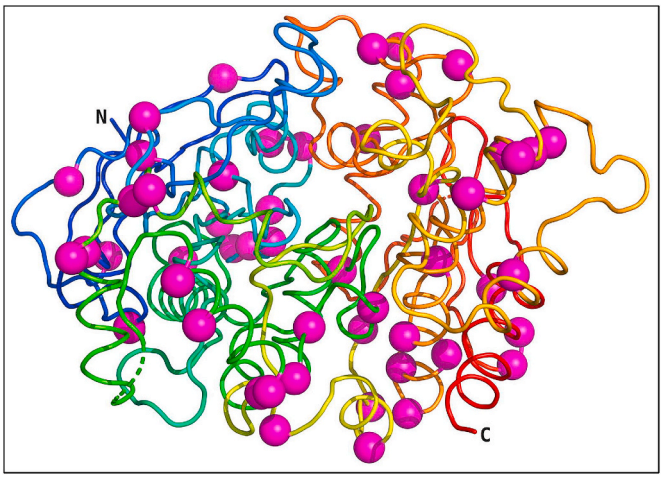

Fig. 1. Crystal structure of a hAChE designed using the PROSS algorithm, and expressed in *E coli*. It is displayed in ribbon form, colored from the N-terminus to the C-terminus in a spectrum going from blue to red. The 51 amino acids that were mutated on the basis of the prediction of the PROSS algorithm are shown as magenta spheres. (For interpretation of the references to color in this figure legend, the reader is referred to the Web version of this article.)

same time excluding the introduction of deleterious mutations, by careful selection of changes that do not introduce any predicted loss of protein stability. This latter feature makes an important contribution to the success achieved by PROSS, since many attempts to generate similar predictive algorithms were not able to avoid deleterious mutations.

The first protein on which PROSS was tested was hAChE. It was selected as the first candidate since, as already mentioned, attempts to express it in an active and soluble form in a prokaryotic expression system had been completely unsuccessful. Application of PROSS to hAChE met with spectacular success. Five design mutants were generated, bearing 17–67 mutations, scattered all over the surface and interior of the enzyme. All these variants expressed well in *E. coli*, producing 2–3 orders of magnitude higher enzymic activity than WT hAChE (whose expression level was so low that it was hard to quantitate), reaching up to 2 mg/ml of AChE protein. They all displayed thermal stability *ca.* 20° higher than WT hAChE expressed in a eukaryotic expression system. Furthermore, they hydrolyzed ACh at rates within 2-fold of the value for WT hAChE, and displayed rate constants for inactivation by the nerve agent VX that are nearly identical to the value for the WT enzyme (Goldenzweig et al., 2016).

The D4AChE design variant, bearing 51 mutations (Fig. 1), was crystallized as its conjugate with the nerve agent VX [PDB-ID 5hq3]. Comparison of the 3D structure of D4AChE to that of WT hAChE revealed an overall RMSD of 0.7 Å over Cα atoms, and atoms in the catalytic gorge aligned particularly well, with an all-atom RMSD of only 0.125 Å. Thus, despite 51 mutations relative to wild-type, ~2000-fold gain in bacterial expression levels, and 20 °C higher heat tolerance, D4AChE is virtually indistinguishable in its active site from WT hAChE. Differences throughout in the structure can be seen online interactively and in 3D at http://proteopedia.org/w/Journal:Molecular_Cell:1). D4AChE thus provides a promising model for use in structural studies of inhibitors that target the AChE active site.

Subsequently, PROSS was successfully applied to expression of hBChE in *E coli* (Brazzolotto et al., 2017). A variant predicted by PROSS, which carries 47 mutations, was expressed at high levels, purified, and crystallized. Again, the designed hBChE had kinetic constants similar to those of the WT enzyme, and its crystal structure revealed that its conformation closely resembled that of the WT enzyme.

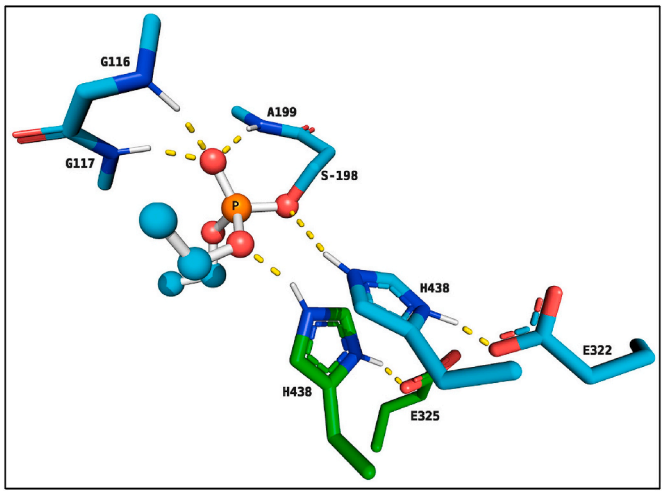

Fig. 2. Change in orientation of the catalytic histidine (H438) in the N322E/E325G mutant. Carbon atoms of H438 and E325 are shown as green sticks for the wild-type conformation. Carbon atoms of H438 and E322, as well as of the oxyanion hole residues - G116, G117 and A199 - are shown as cyan sticks for the mutant. In both cases, oxygens are coded in red, and nitrogens in blue. The OP moiety covalently attached to S198 in the mutant is displayed as balls, with the phosphorus in orange, the oxygens in red and the carbons in cyan. H-bonds are shown as yellow dashed lines. (For interpretation of the references to color in this figure legend, the reader is referred to the Web version of this article.)

4. Computer-designed human butyrylcholinesterase possessing a new catalytic triad

Lockridge and coworkers showed that a single mutation, G117H, conferred phosphotriesterase activity on hBChE (Lockridge et al., 1997). The mutant enzyme was able to hydrolyse both echothiophate and paraoxon. Subsequent crystallographic studies showed that formation of the phosphyl adducts of the mutant enzyme was accompanied by a shift in the position of H117 that offered a plausible mechanism for its involvement in the dephosphylation step (Nachon et al., 2011).

The impressive growth in the power of computer design to successfully predict the outcome of specific mutations is elegantly illustrated in a recent study on the engineering of hBChE (Grigorenko et al., 2019). In this study, *in silico* modeling predicted that in the N322E/E325G double mutant the catalytic triad of WT hBChE, S198–H438-E325, would be replaced by a novel catalytic triad - S198–H438-E322 (Fig. 2). Furthermore, MD simulations predicted that the mutant enzyme should be catalytically active, and also interact covalently with the OP, echothiophate.

A monomeric form of the N322E/E325G double mutant was expressed in HEK cells, and shown to be catalytically active on butyrylthiocholine. Furthermore, like the WT enzyme, it was inactivated by echothiophate. Again, like WT hBChE, the OP conjugate slowly reactivated spontaneously, but the qualitative data generated do not permit a decision as to whether reactivation of the double mutant is slower or faster than that of the WT.

5. A dynamic basis for the differential activity on mammalian and electric organ AChEs of the covalent inhibitor phenymethylsulfonyl fluoride (PMSF)

Phenylmethylsulfonyl fluoride (PMSF) is a covalent inhibitor of serine hydrolases commonly used in the preparation of cell lysates (Le et al., 2015). It has long been known that it inhibits *Ee*AChE very poorly (Fahrney and Gold, 1963), even though it inhibits mammalian AChEs very well (Moss and Fahrney, 1978). More recently, it was shown that PMSF also inhibits *Tc*AChE very poorly (Kraut et al., 2000a). However, it was also observed that benzylsulfonyl fluoride (BSF) inhibits both

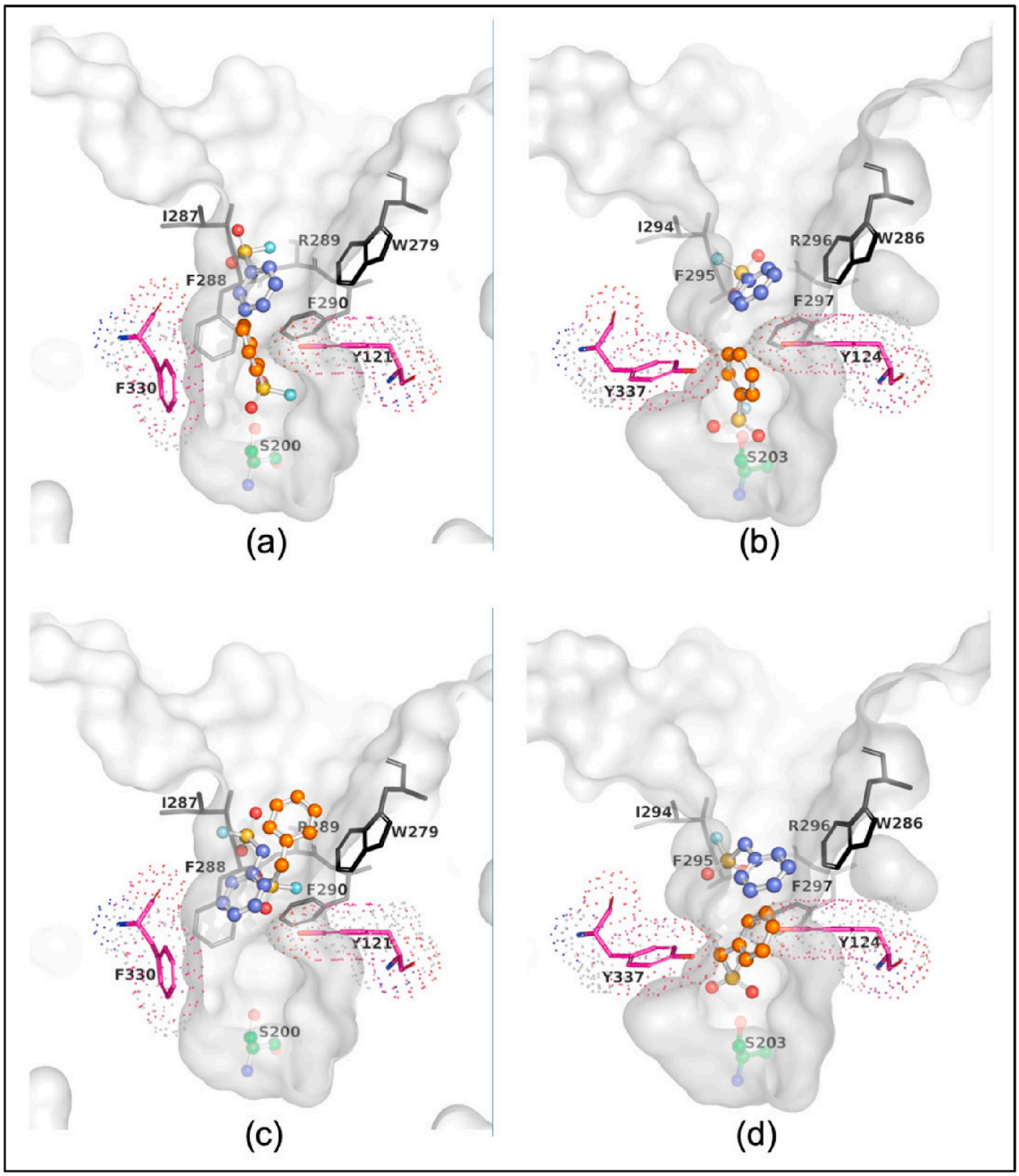

Fig. 3. Docking and MD simulations for interaction of BSF and PMSF with *Tc*AChE and mAChE. The upper panels show the data obtained for interaction of BSF with (a) *Tc*AChE and (b) mAChE. The lower panels show the data obtained for interaction of PMSF with (c) *Tc*AChE and (d) mAChE. In all four panels two copies of the ligand are displayed. One shows the position of the ligand after docking alone (blue), and the other shows the position after docking followed by MD simulation (orange). It should be noted that the orientations of the amino-acid side-chains displayed are those seen prior to the MD simulations. (For interpretation of the references to color in this figure legend, the reader is referred to the Web version of this article.)

*Tc*AChE and mAChE very well. These were puzzling observations, since the only difference between BSF and PMSF is the methylene group between the benzene ring and the sulfonyl moiety in the latter. Moreover, the catalytic activity of mammalian and electric organ AChE on ACh and acetylthiocholine is very similar (Vigny et al., 1978).

In a theoretical study that combined ligand docking with a subsequent MD protocol (Chandar et al., 2019), it was shown that both in mAChE and *Tc*AChE BSF passes through the bottleneck within the active-site gorge, and approaches the catalytic triad. However, whereas PMSF can pass through the bottleneck in mAChE, it is not able to do so in *Tc*AChE (Fig. 3). MD simulations on the native enzyme structures revealed that mAChE is substantially more flexible than *Tc*AChE, suggesting that enhanced 'breathing motions' of the mouse enzyme, relative to the *Torpedo* enzyme, may explain why PMSF can pass through the bottleneck in the former, but not in the latter. The difference between PMSF and BSF may tentatively be ascribed to the fact that BSF is planar, whereas PMSF is not.

Experimental data are also consistent with the notion that breathing motions or conformational flexibility are involved in controlling access of PMSF to the active site. Thus, mutating two aromatic residues in the acyl pocket (F288L/F290V), thereby enabling *Tc*AChE to hydrolyse butrylthiocholine (Harel et al., 1992), also greatly enhances its rate of inhibition by PMSF (Kraut et al., 2000a). Furthermore, the L282A mutant, which is less stable than the WT enzyme (Morel et al., 1999), is

inhibited by PMSF at a rate similar to that at which the double mutant is inhibited (Kraut et al., 2000b).

PMSF is not the only covalent reagent for which very different reactivity towards mammalian AChEs and *Tc*AChE is observed. Rivastigmine is a carbamate inhibitor of AChE which, under the trade name Exelon®, is used for treatment of Alzheimer's disease (Enz et al., 1993). Rivastigmine inhibits *Tc*AChE with a bimolecular rate constant 1600-fold lower than that at which it inhibits the human enzyme (Bar-On et al., 2002). It contains a bulky leaving group that may account for this difference, but no MD studies have been performed to support this possibility.

However, various organophosphates (OPs) do not differ greatly in their rates of phosphorylation of *Tc*AChE and hAChE. Thus, the two enzymes are inhibited at quite similar rates by diisopropylphosphorofluoridate (DFP) (Millard et al., 1999). Another interesting case for comparison is that of the alkaloid, (−)-huperzine A (HupA). HupA is a bulky molecule with a rigid structure and a diameter of 9.8 Å. Although HupA is a reversible inhibitor, it inhibits AChE extremely slowly, and its rate of disassociation is also very low (Ashani et al., 1994). MD and steered MD simulations show that sizeable distortions of the residues along the active-site gorge are required for it to pass the bottleneck (Bai et al., 2013; Rydzewski et al., 2018; Xu et al., 2003). Yet the rates of inhibition of *Tc*AChE and hAChE by HupA are very similar (Ashani et al., 1994). Furthermore, many bulky and/or gorge-spanning ligands, such as galanthamine (Greenblatt et al., 1999) and E2020 (Kryger et al., 1999), interact with AChE, and disassociate from it, very rapidly. It is obvious that our understanding of how protein function is coupled to protein dynamics in the ChEs is inadequate, to say the least.

6. Microsecond MD studies of domain motions of AChE

In the previous section we used docking, together with MD simulations, to study how the covalent inhibitors, PMSF and BSF, move through the bottleneck midway down the gorge in mouse and *Torpedo* AChE, and showed how the flexibility of the enzymes, as reflected in their 'breathing' motions, affects the movement of the inhibitors (Chandar et al., 2019). Most of these simulations were of only 20 ns duration. However, as mentioned in the Introduction, computing power is increasing continuously. In a recent study, microsecond MD simulations were used to study subdomain movements and breathing motions of the gorge in *Tc*AChE (Cheng et al., 2017). Surprisingly, it was observed that not only amino acid residues lining and adjacent to the gorge, but also distant residues, appear to be tightly associated with changes in the gorge radius, and thus contribute to the 'breathing' motions of the active-site gorge. Thus, long-range 'communication', via multiple residue-residue interactions, may rationalize the influence of remote residues on those lining the gorge.

Not only were the dynamics of the monomer studied, but also those of its complex with a gorge-spanning inhibitor, the anti-Alzheimer drug, E2020, as well as the complete physiological dimer. The functional forms of AChE at cholinergic synapses are all oligomeric. Thus, it is important to understand to what extent oligomerization affects the dynamics of the monomer. Dynamics of three subdomains were studied, including that of the Ω-loop, which bears the W84 residue in the CAS with which the quaternary group of ACh interacts. High correlation was observed in the movements of these subdomains. This correlation lies at the basis of the capacity of remote residues to modulate breathing motions of the gorge allosterically.

7. Reassessment of existing crystal structures yields novel information

Structural biology is an example of an experimental discipline in which both the experimental and computational technologies have developed enormously over the past thirty years. Thus, at the experimental level, it is now possible to collect complete data sets at synchrotrons in a few minutes, rather than over a period of several hours, as was the case in the early 1990s. However, this is also true for analysis of the experimental data, due primarily to developments in the CCP4 Suite of programs (Winn et al., 2011), such as REFMAC (Murshudov et al., 1997) for refinement, COOT (Emsley et al., 2010) for fitting molecules to electron density, and the PHENIX package (Liebschner et al., 2019) for refinement. Fortunately, in many cases, the X-ray structure factors are retained in the PDB, and the original data frames are often preserved at the synchrotrons where they were collected. It is thus possible to reexamine the data taking advantage of the major improvements in software (see above) in order to find out: a) If more accurate structures can be obtained, in which features of the experimental map can be better assigned; b) Whether, as a consequence, structure-function relationships can be better understood. Automated post-deposition optimization, utilizing PDB_REDO often generates significant improvements in X-ray structure models (Touw et al., 2016).

Two examples of such reexaminations have recently been published: 1) A reexamination of the complex of methylene blue with *Tc*AChE (Dym et al., 2016), originally described in 2012 (Paz et al., 2012); 2) A reexamination of the 3D structure of *Dm*AChE, and of its complexes with tacrine derivatives (Nachon et al., 2020), originally described 20 years earlier (Harel et al., 2000).

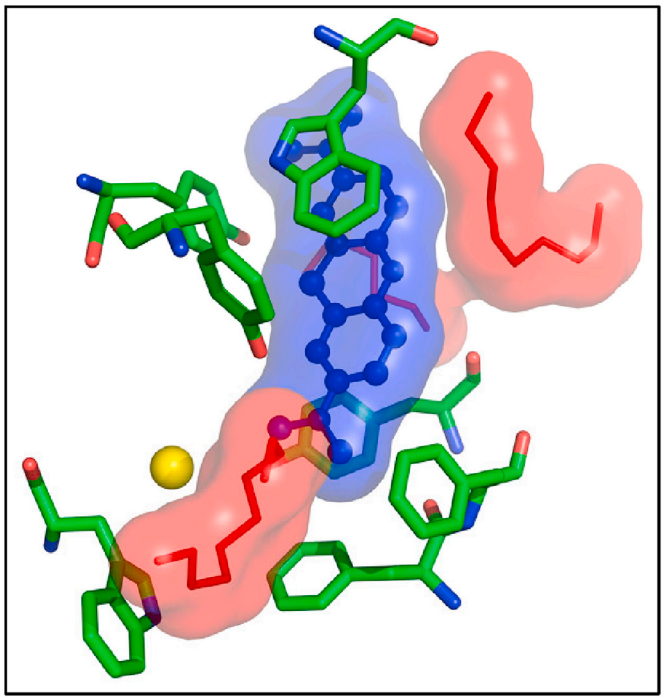

Fig. 4. Effect of ethylene glycol oligomers (PEGs) on the positioning of the ligand in the crystal structure of the methylene blue/*Tc*AChE complex crystallized from PEG200. Three PEGs are shown in red, methylene blue in blue, and conserved aromatic residues lining the active-site gorge in green. A highly conserved H_2O molecule, shown as a yellow sphere, also affects the positioning of the ligand. (For interpretation of the references to color in this figure legend, the reader is referred to the Web version of this article.)

8. The methylene blue/TcAChE complex

Structure-based drug design utilizes apo protein or complex structures retrieved from the PDB. More than 57% of the crystallographic PDB entries were obtained with polyethylene glycols (PEGs) as precipitant and/or as cryoprotectant, but *less than 6%* of these entries display individual ethylene glycol oligomers in the refined structures (Dym et al., 2016)! In complexes of *Tc*AChE with methylene blue and decamethonium, the presence of ethylene glycol oligomers in the crystal

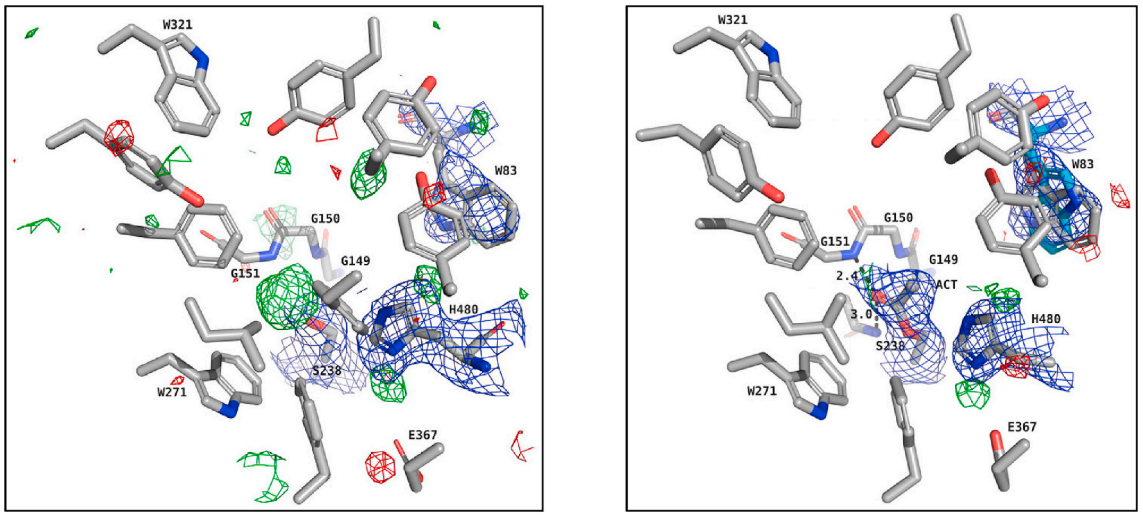

Fig. 5. Active-site gorge in the original (left) and updated (right) structures of native *Dm*AChE. Residues of the catalytic triad (E367/H480/S238), of the oxyanion hole (G150/G151/Al239), and key residues of the peripheral site (W321), acyl-binding pocket (W271), and choline-binding pocket (W83), are represented as sticks, with carbons in white, nitrogens in blue, and oxygens in red. The alternative conformation of W83 is depicted with carbons in cyan. The acetyl (ACT) is represented as balls and sticks. H-bonds are depicted as black dashes, with distances in Å. The meshes represent the 2 |Fo| – |Fc| map (1 σ blue) and the |Fo| – |Fc| difference map (3 σ green/−3 σ red). (For interpretation of the references to color in this figure legend, the reader is referred to the Web version of this article.)

structure markedly affected the positioning of the bound ligand (Dym et al., 2016). Isomorphous crystals were obtained of complexes of both ligands, using either ammonium sulfate or PEG200 as the precipitant. In the complexes obtained using crystals precipitated with ammonium sulfate, both methylene blue and decamethonium make direct π-cation interactions with the indole ring of W84, in the CAS, as is typical of quaternary inhibitors of AChE (Harel et al., 1993, 1996). In the crystals obtained by precipitation with PEG200, in both cases an ethylene glycol oligomer is seen bound to W84, in a mode similar to that earlier described for a PEG molecule bearing a thiol group (Koellner et al., 2002), thus preventing interaction of the ligands' proximal quaternary groups with its indole group. As a consequence, both methylene blue (Fig. 4) and decamethonium are positioned ~3.0 Å further up the gorge, making stronger interactions with W279 in the PAS. These findings have cogent implications for structure-based drug design, since data obtained for complexes obtained when a PEG is employed as the precipitant may not reflect the ligand's position in its absence, and could thus result in selection of incorrect leads for drug discovery. Indeed, docking methylene blue into the crystal structure obtained with PEG200, but omitting the ethylene glycols, yields results agreeing poorly with the crystal structure, whereas excellent agreement is obtained if they are included (Dym et al., 2016). Many proteins display features in which precipitants might lodge. Thus, it is crucial to investigate the presence of precipitants in published crystal structures, so as to check whether their presence has resulted in misinterpretation of the electron density maps, thus adversely affecting drug design.

9. Reexamination of the DmAChE crystal structure

Over recent decades, crystallographic software for data processing and structure refinement has improved dramatically, resulting in more accurate and detailed crystal structures. It is, therefore, sometimes valuable to have a second look at "old" diffraction data, especially when earlier interpretation of the electron density maps was rather difficult. Recently this was done for the crystal structures of *Drosophila melanogaster* acetylcholinesterase (*Dm*AChE), originally published in 2000 (Harel et al., 2000), which revealed features that had not been noticed earlier (Fig. 5). Thus, previously un-modeled density in the native active site can be interpreted as stable acetylation of the catalytic serine. Similarly, a strong density in the *Dm*AChE/ZA complex, originally attributed to a sulfate ion, is better interpreted as a small molecule that is covalently bound. This small molecule can be modeled as either a propionate or a glycinate. The complex is reminiscent of the carboxylate/BChE complexes observed in crystal structures of hBChE (Brazzolotto et al., 2012; Nicolet et al., 2003), and demonstrates the remarkable ability of ChEs to stabilize covalent complexes with carboxylates. A very strong peak of density (10 σ) at covalent distance from the Cβ atom of the catalytic serine is present in the *Dm*AChE/ZAI complex. This can be undoubtedly attributed to an iodine atom, suggesting an unanticipated iodo/hydroxyl exchange between S238 and the inhibitor, possibly caused by the intense synchrotron X-ray irradiation. Finally, the binding of tacrine-derived inhibitors, such as ZA (1DX4) or the iodinated analog, ZAI (1QON), results in the appearance of an open channel that connects the base of the active-site gorge to the solvent, as originally noticed by Nachon and coworkers (Nachon et al., 2008). This channel, which arises due to the absence of the conserved tyrosine present in vertebrate ChEs, has the potential to be exploited for the design of inhibitors specific to insect ChEs. Overall, the study demonstrates that updated processing of older diffraction images, and the re-refinement of older diffraction data, can produce valuable information that would have been difficult or impossible to detect in the original analysis, and strongly supports preservation of the diffraction images in public data banks.

10. Concluding remarks

In the above, we have surveyed some recent studies in order to illustrate how application of cutting edge computational techniques can: (a) Heighten our understanding of how the ChEs function; (b) Design variants engineered to improve, or otherwise modulate, their function; (c) Improve approaches to the design of leads for novel ChE inhibitors. As already noted above, our understanding of the relationship of the dynamics of the ChEs to their activity is a topic that demands especial attention.

Declaration of competing interest

No conflict of interest.

References

Ashani, Y., Grunwald, J., Kronman, C., Velan, B., Shafferman, A., 1994. Role of tyrosine 337 in the binding of huperzine A to the active site of human acetylcholinesterase. Mol. Pharmacol. 45, 555–560.

Bai, F., Xu, Y., Chen, J., Liu, Q., Gu, J., Wang, X., Ma, J., Li, H., Onuchic, J.N., Jiang, H., 2013. Free energy landscape for the binding process of Huperzine A to acetylcholinesterase. Proc. Natl. Acad. Sci. U.S.A. 110, 4273–4278. https://doi.org/10.1073/pnas.1301814110.

Bar-On, P., Millard, C.B., Harel, M., Dvir, H., Enz, A., Sussman, J.L., Silman, I., 2002. Kinetic and structural studies on the interaction of cholinesterases with the anti-Alzheimer drug rivastigmine. Biochemistry 41, 3555–3564. https://doi.org/10.1021/bi020016x.

Bazelyansky, M., Robey, C., Kirsch, J.F., 1986. Fractional diffusion-limited component of reactions catalyzed by acetylcholinesterase. Biochemistry 25, 125–130. https://doi.org/10.1021/bi00349a019.

Botti, S.A., Felder, C., Lifson, S., Sussman, J.L., Silman, I., 1999. A modular treatment of molecular traffic through the active site of cholinesterases. Biophys. J. 77, 2430–2450. https://doi.org/10.1016/S0006-3495(99)77080-3.

Bourne, Y., Grassi, J., Bougis, P.E., Marchot, P., 1999. Conformational flexibility of the acetylcholinesterase tetramer suggested by X-ray crystallography. J. Biol. Chem. 274, 30370–30376. https://doi.org/10.1074/jbc.274.43.30370.

Bourne, Y., Radic, Z., Sulzenbacher, G., Kim, E., Taylor, P., Marchot, P., 2006. Substrate and product trafficking through the active center gorge of acetylcholinesterase analyzed by crystallography and equilibrium binding. J. Biol. Chem. 281, 29256–29267. https://doi.org/10.1074/jbc.M603018200.

Bourne, Y., Renault, L., Marchot, P., 2015. Crystal structure of snake venom acetylcholinesterase in complex with inhibitory antibody fragment Fab410 bound at the peripheral site: evidence for open and closed states of a backdoor channel. J. Biol. Chem. 290, 1522–1535. https://doi.org/10.1074/jbc.M114.603902.

Bourne, Y., Taylor, P., Marchot, P., 1995. Acetylcholinesterase inhibition by fasciculin: crystal structure of the complex. Cell 83, 503–512. https://doi.org/10.1016/0092-8674(95)90128-0.

Brazzolotto, X., Igert, A., Guillon, V., Santoni, G., Nachon, F., 2017. Bacterial expression of human butyrylcholinesterase as a tool for nerve agent bioscavengers development. Molecules 22, 1828. https://doi.org/10.3390/molecules22111828.

Brazzolotto, X., Wandhammer, M., Ronco, C., Trovaslet, M., Jean, L., Lockridge, O., Renard, P.-Y., Nachon, F., 2012. Human butyrylcholinesterase produced in insect cells: huprine-based affinity purification and crystal structure. FEBS J. 279, 2905–2916. https://doi.org/10.1111/j.1742-4658.2012.08672.x.

Chandar, N.B., Efremenko, I., Silman, I., Martin, J.M.L., Sussman, J.L., 2019. Molecular dynamics simulations of the interaction of mouse and *Torpedo* acetylcholinesterase with covalent inhibitors explain their differential reactivity: implications for drug design. Chem. Biol. Interact. 310, 108715. https://doi.org/10.1016/j.cbi.2019.06.028.

Cheng, S., Song, W., Yuan, X., Xu, Y., 2017. Gorge motions of acetylcholinesterase revealed by microsecond molecular dynamics simulations. Sci. Rep. 7, 3219. https://doi.org/10.1038/s41598-017-03088-y.

Cheung, J., Mahmood, A., Kalathur, R., Liu, L., Carlier, P.R., 2018. Structure of the G119S mutant acetylcholinesterase of the malaria vector *Anopheles gambiae* reveals basis of insecticide resistance. Structure 26, 130–136. https://doi.org/10.1016/j.str.2017.11.021.

Cheung, J., Rudolph, M.J., Burshteyn, F., Cassidy, M.S., Gary, E.N., Love, J., Franklin, M.C., Height, J.J., 2012. Structures of human acetylcholinesterase in complex with pharmacologically important ligands. J. Med. Chem. 55, 10282–10286. https://doi.org/10.1021/jm300871x.

Colletier, J.P., Fournier, D., Greenblatt, H.M., Stojan, J., Sussman, J.L., Zaccai, G., Silman, I., Weik, M., 2006. Structural insights into substrate traffic and inhibition in acetylcholinesterase. EMBO J. 25, 2746–2756. https://doi.org/10.1038/sj.emboj.7601175.

Dym, O., Song, W., Felder, C., Roth, E., Shnyrov, V., Ashani, Y., Xu, Y., Joosten, R.P., Weiner, L., Sussman, J.L., Silman, I., 2016. The impact of crystallization conditions on structure-based drug design: a case study on the methylene blue/acetylcholinesterase complex. Protein Sci. 25, 1096–1114. https://doi.org/10.1002/pro.2923.

Emsley, P., Lohkamp, B., Scott, W.G., Cowtan, K., 2010. Features and development of coot. Acta Crystallogr. Sect. D Biol. Crystallogr. 66, 486–501. https://doi.org/10.1107/S0907444910007493.

Enz, A., Amstutz, R., Boddeke, H., Gmelin, G., Malanowski, J., 1993. Brain selective inhibition of acetylcholinesterase: a novel approach to therapy for Alzheimer's disease. Prog. Brain Res. 98, 431–438. https://doi.org/10.1016/s0079-6123(08)62429-2.

Fahrney, D.E., Gold, A.M., 1963. Sulfonyl fluorides as inhibitors of esterases. I. Rates of reaction with acetylcholinesterase, alpha-chymotrypsin and trypsin. J. Am. Chem. Soc. 85, 997–1000. https://doi.org/10.1021/ja00890a037.

Felder, C.E., Botti, S.A., Lifson, S., Silman, I., Sussman, J.L., 1997. External and internal electrostatic potentials of cholinesterase models. J. Mol. Graph. Model. 15 (318–327), 335–337. https://doi.org/10.1016/s1093-3263(98)00005-9.

Fischer, M., Ittah, A., Gorecki, M., Werber, M.M., 1995. Recombinant human acetylcholinesterase expressed in *Escherichia coli*: refolding, purification and characterization. Biotechnol. Appl. Biochem. 21, 295–311. https://doi.org/10.1111/j.1470-8744.1995.tb00337.x.

Friesner, R.A., Banks, J.L., Murphy, R.B., Halgren, T.A., Klicic, J.J., Mainz, D.T., Repasky, M.P., Knoll, E.H., Shelley, M., Perry, J.K., Shaw, D.E., Francis, P., Shenkin, P.S., 2004. Glide: A new approach for rapid, accurate docking and scoring. 1. Method and assessment of docking accuracy. J. Med. Chem. 47, 1739–1749. https://doi.org/10.1021/jm0306430.

Friesner, R.A., Murphy, R.B., Repasky, M.P., Frye, L.L., Greenwood, J.R., Halgren, T.A., Sanschagrin, P.C., Mainz, D.T., 2006. Extra precision glide: docking and scoring incorporating a model of hydrophobic enclosure for protein-ligand complexes. J. Med. Chem. 49, 6177–6196. https://doi.org/10.1021/jm051256o.

Fuxreiter, M. (Ed.), 2015. Computational Approaches to Protein Dynamics: from Quantum to Coarse-Grained Methods. CRC Press, Boca Raton. https://doi.org/10.1201/b17979.

Gilson, M.K., Straatsma, T.P., McCammon, J.A., Ripoll, D.R., Faerman, C.H., Axelsen, P.H., Silman, I., Sussman, J.L., 1994. Open "back door" in a molecular dynamics simulation of acetylcholinesterase. Science 263, 1276–1278. https://doi.org/10.1126/science.8122110.

Goldenzweig, A., Goldsmith, M., Hill, S.E., Gertman, O., Laurino, P., Ashani, Y., Dym, O., Unger, T., Albeck, S., Prilusky, J., Lieberman, R.L., Aharoni, A., Silman, I., Sussman, J.L., Tawfik, D.S., Fleishman, S.J., 2016. Automated structure- and sequence-based design of proteins for high bacterial expression and stability. Mol. Cell. 63, 337–346. https://doi.org/10.1016/j.molcel.2016.06.012.

Goodsell, D.S., Morris, G.M., Olson, A.J., 1996. Automated docking of flexible ligands: applications of AutoDock. J. Mol. Recogn. 9, 1–5. https://doi.org/10.1002/(SICI)1099-1352(199601)9:1<1::AID-JMR241>3.0.CO;2-6.

Greenblatt, H.M., Kryger, G., Lewis, T., Silman, I., Sussman, J.L., 1999. Structure of acetylcholinesterase complexed with (-)-galanthamine at 2.3 Å resolution. FEBS Lett. 463, 321–326. https://doi.org/10.1016/s0014-5793(99)01637-3.

Grigorenko, B.L., Novichkova, D.A., Lushchekina, S.V., Zueva, I.V., Schopfer, L.M., Nemukhin, A.V., Varfolomeev, S.D., Lockridge, O., Masson, P., 2019. Computer-designed active human butyrylcholinesterase double mutant with a new catalytic triad. Chem. Biol. Interact. 306, 138–146. https://doi.org/10.1016/j.cbi.2019.04.019.

Halgren, T.A., Murphy, R.B., Friesner, R.A., Beard, H.S., Frye, L.L., Pollard, W.T., Banks, J.L., 2004. Glide: A new approach for rapid, accurate docking and scoring. 2. enrichment factors in database screening. J. Med. Chem. 47, 1750–1759. https://doi.org/10.1021/jm030644s.

Han, Q., Wong, D.M., Robinson, H., Ding, H., Lam, P.C.H., Totrov, M.M., Carlier, P.R., Li, J., 2018. Crystal structure of acetylcholinesterase catalytic subunits of the malaria vector *Anopheles gambiae*. Insect Sci. 25, 721–724. https://doi.org/10.1111/1744-7917.12450.

Harel, M., Kryger, G., Rosenberry, T.L., Mallender, W.D., Lewis, T., Fletcher, R.J., Guss, J.M., Silman, I., Sussman, J.L., 2000. Three-dimensional structures of *Drosophila melanogaster* acetylcholinesterase and of its complexes with two potent inhibitors. Protein Sci. 9, 1063–1072. https://doi.org/10.1110/ps.9.6.1063.

Harel, M., Quinn, D.M., Nair, H.K., Silman, I., Sussman, J.L., 1996. The X-ray structure of a transition state analog complex reveals the molecular origins of the catalytic power and substrate specificity of acetylcholinesterase. J. Am. Chem. Soc. 118, 2340–2346. https://doi.org/10.1021/ja952232h.

Harel, M., Schalk, I., Ehret-Sabatier, L., Bouet, F., Goeldner, M., Hirth, C., Axelsen, P., Silman, I., Sussman, J.L., 1993. Quaternary ligand binding to aromatic residues in the active-site gorge of acetylcholinesterase. Proc. Natl. Acad. Sci. U.S.A. 90, 9031–9035. https://doi.org/10.1073/pnas.90.19.9031.

Harel, M., Sussman, J.L., Krejci, E., Bon, S., Chanal, P., Massoulié, J., Silman, I., 1992. Conversion of acetylcholinesterase to butyrylcholinesterase: modeling and mutagenesis. Proc. Natl. Acad. Sci. U.S.A. 89, 10827–10831. https://doi.org/10.1073/pnas.89.22.10827.

Heim, J., Schmidt-Dannert, C., Atomi, H., Schmid, R.D., 1998. Functional expression of a mammalian acetylcholinesterase in *Pichia pastoris*: comparison to acetylcholinesterase, expressed and reconstituted from *Escherichia coli*. Biochim. Biophys. Acta 1396, 306–319. https://doi.org/10.1016/s0167-4781(97)00196-6.

Hulme, E.C., Lu, Z.L., Saldanha, J.W., Bee, M.S., 2003. Structure and activation of muscarinic acetylcholine receptors. Biochem. Soc. Trans. 31, 29–34. https://doi.org/10.1042/bst0310029.

Jones, G., Willett, P., Glen, R.C., 1995. Molecular recognition of receptor sites using a genetic algorithm with a description of desolvation. J. Mol. Biol. 245, 43–53. https://doi.org/10.1016/s0022-2836(95)80037-9.

Jones, G., Willett, P., Glen, R.C., Leach, A.R., Taylor, R., 1997. Development and validation of a genetic algorithm for flexible docking. J. Mol. Biol. 267, 727–748. https://doi.org/10.1006/jmbi.1996.0897.

Koellner, G., Kryger, G., Millard, C.B., Silman, I., Sussman, J.L., Steiner, T., 2000. Active-site gorge and buried water molecules in crystal structures of acetylcholinesterase from *Torpedo californica*. J. Mol. Biol. 296, 713–735. https://doi.org/10.1006/jmbi.1999.3468.

Koellner, G., Steiner, T., Millard, C.B., Silman, I., Sussman, J.L., 2002. A neutral molecule in a cation-binding site: specific binding of a PEG-SH to acetylcholinesterase from *Torpedo californica*. J. Mol. Biol. 320, 721–725. https://doi.org/10.1016/s0022-2836(02)00475-8.

Kraut, D., Goff, H., Pai, R.K., Hosea, N.A., Silman, I., Sussman, J.L., Taylor, P., Voet, J.G., 2000a. Inactivation studies of acetylcholinesterase with phenylmethanesulfonyl fluoride. Mol. Pharmacol. 57, 1243–1248.

Kraut, D., Morel, N., Bon, S., Massoulié, J., Silman, I., Sussman, J.L., Voet, J.G., 2000b. *Torpedo* AChE L282A mutant (destabilized) becomes PMSF sensitive. Biochemistry 39, 1547. https://doi.org/10.1021/bi9950995.

Kryger, G., Harel, M., Giles, K., Toker, L., Velan, B., Lazar, A., Kronman, C., Barak, D., Ariel, N., Shafferman, A., Silman, I., Sussman, J.L., 2000. Structures of recombinant native and E202Q mutant human acetylcholinesterase complexed with the snake-venom toxin fasciculin-II. Acta Crystallogr. Sect. D Biol. Crystallogr. 56, 1385–1394. https://doi.org/10.1107/s0907444900010659.

Kryger, G., Silman, I., Sussman, J.L., 1999. Structure of acetylcholinesterase complexed with E2020 (Aricept): implications for the design of new anti-Alzheimer drugs. Structure 7, 297–307. https://doi.org/10.1016/s0969-2126(99)80040-9.

Le, T., Lee, H.J., Jin, H.J., 2015. An efficient method to eliminate the protease activity contaminating commercial bovine pancreatic DNase I. Anal. Biochem. 483, 4–6. https://doi.org/10.1016/j.ab.2015.04.030.

Liebschner, D., Afonine, P.V., Baker, M.L., Bunkoczi, G., Chen, V.B., Croll, T.I., Hintze, B., Hung, L.W., Jain, S., McCoy, A.J., Moriarty, N.W., Oeffner, R.D., Poon, B.K., Prisant, M.G., Read, R.J., Richardson, J.S., Richardson, D.C., Sammito, M.D., Sobolev, O.V., Stockwell, D.H., Terwilliger, T.C., Urzhumtsev, A.G., Videau, L.L., Williams, C.J., Adams, P.D., 2019. Macromolecular structure determination using X-rays, neutrons and electrons: recent developments in Phenix. Acta Crystallogr. Sect. D Biol. Crystallogr. 75, 861–877. https://doi.org/10.1107/S2059798319011471.

Lockridge, O., Blong, R.M., Masson, P., Froment, M.-T., Millard, C.B., Broomfield, C.A., 1997. A single amino acid substitution, Gly117His, confers phosphotriesterase (organophosphorus acid anhydride hydrolase) activity on human butyrylcholinesterase. Biochemistry 36, 786–795. https://doi.org/10.1021/bi961412g.

Lushchekina, S.V., Schopfer, L.M., Grigorenko, B.L., Nemukhin, A.V., Varfolomeev, S.D., Lockridge, O., Masson, P., 2018. Optimization of cholinesterase-based catalytic bioscavengers against organophosphorus agents. Front. Pharmacol. 9, 211. https://doi.org/10.3389/fphar.2018.00211.

Masson, P., Adkins, S., Pham-Trong, P., Lockridge, O., 1992. Expression and refolding of functional human butyrylcholinesterase from E. coli. In: Shafferman, A., Velan, B. (Eds.), Multidisciplinary Approaches to Cholinesterase Functions. Springer, Boston, MA, pp. 49–52. https://doi.org/10.1007/978-1-4615-3046-6_6.

Masson, P., Froment, M.T., Bartels, C.F., Lockridge, O., 1996. Asp7O in the peripheral anionic site of human butyrylcholinesterase. Eur. J. Biochem. 235, 36–48. https://doi.org/10.1111/j.1432-1033.1996.00036.x.

Maxwell, D.M., Saxena, A., Gordon, R.K., Doctor, B.P., 1999. Improvements in scavenger protection against organophosphorus agents by modification of cholinesterases. Chem. Biol. Interact. 119–120, 419–428. https://doi.org/10.1016/s0009-2797(99)00054-x.

Millard, C.B., Kryger, G., Ordentlich, A., Greenblatt, H.M., Harel, M., Raves, M.L., Segall, Y., Barak, D., Shafferman, A., Silman, I., Sussman, J.L., 1999. Crystal structures of aged phosphonylated acetylcholinesterase: nerve agent reaction products at the atomic level. Biochemistry 38, 7032–7039. https://doi.org/10.1021/bi982678l.

Morel, N., Bon, S., Greenblatt, H.M., Van Belle, D., Wodak, S.J., Sussman, J.L., Massoulié, J., Silman, I., 1999. Effect of mutations within the peripheral anionic site on the stability of acetylcholinesterase. Mol. Pharmacol. 55, 982–992. https://doi.org/10.1124/mol.55.6.982.

Moss, D.E., Fahrney, D.E., 1978. Kinetic analysis of differences in brain acetylcholinesterase from fish or mammalian sources. Biochem. Pharmacol. 27, 2693–2698. https://doi.org/10.1016/0006-2952(78)90044-8.

Mukhametgalieva, A.R., Aglyamova, A.R., Lushchekina, S.V., Golicnik, M., Masson, P., 2019. Time-course of human cholinesterases-catalyzed competing substrate kinetics. Chem. Biol. Interact. 310, 108702. https://doi.org/10.1016/j.cbi.2019.06.015.

Murshudov, G., Vagin, A., Dodson, E., 1997. Refinement of macromolecular structures by the maximum-likelihood method. Acta Crystallogr. Sect. D Biol. Crystallogr. 53, 240–255. https://doi.org/10.1107/S0907444996012255.

Nachon, F., Carletti, E., Wandhammer, M., Nicolet, Y., Schopfer, L.M., Masson, P., Lockridge, O., 2011. X-ray crystallographic snapshots of reaction intermediates in the G117H mutant of human butyrylcholinesterase, a nerve agent target engineered into a catalytic bioscavenger. Biochem. J. 434, 73–82. https://doi.org/10.1042/bj20101648.

Nachon, F., Rosenberry, T.L., Silman, I., Sussman, J.L., 2020. A decond look at the crystal structures of *Drosophila melanogaster* acetylcholinesterase in complex with tacrine derivatives provides Insights concerning catalytic intermediates and the design of specific insecticides. Molecules 25, 1198. https://doi.org/10.3390/molecules25051198.

Nachon, F., Stojan, J., Fournier, D., 2008. Insights into substrate and product traffic in the *Drosophila melanogaster* acetylcholinesterase active site gorge by enlarging a back channel. FEBS J. 275, 2659–2664. https://doi.org/10.1111/j.1742-4658.2008.06413.x.

Nicolet, Y., Lockridge, O., Masson, P., Fontecilla-Camps, J.C., Nachon, F., 2003. Crystal structure of human butyryl cholinesterase and of its complexes with substrate and products. J. Biol. Chem. 278, 41141–41147. https://doi.org/10.1074/jbc.M210241200.

Paz, A., Roth, E., Ashani, Y., Xu, Y., Shnyrov, V.L., Sussman, J.L., Silman, I., Weiner, L., 2012. Structural and functional characterization of the interaction of the photosensitizing probe methylene blue with *Torpedo californica* acetylcholinesterase. Protein Sci. 21, 1138–1152. https://doi.org/10.1002/pro.2101.

Porschke, D., Créminon, C., Cousin, X., Bon, C., Sussman, J.L., Silman, I., 1996. Electrooptical measurements demonstrate a large permanent dipole moment associated with acetylcholinesterase. Biophys. J. 70, 1603–1608. https://doi.org/10.1016/S0006-3495(96)79759-X.

Post, M.R., Tender, G.S., Lester, H.A., Dougherty, D.A., 2017. Secondary ammonium agonists make dual cation-pi interactions in α4β2 nicotinic receptors. eNeuro 4. https://doi.org/10.1523/ENEURO.0032-17.2017.

Raves, M., Giles, K., Schrag, J.D., Schmid, M.F., Phillips, G.N., Chiu, W., Howard, A.J., Silman, I., Sussman, J.L., 1998. Quaternary structure of tetrameric acetylcholinesterase. In: Doctor, B.P., Taylor, P., Quinn, D.M., Rotundo, R.L., Gentry, M.K. (Eds.), Structure and Function of Cholinesterases and Related Proteins. Plenum, New York, pp. 351–356. https://doi.org/10.1007/978-1-4899-1540-5_97.

Ripoll, D.R., Faerman, C.H., Axelsen, P.H., Silman, I., Sussman, J.L., 1993. An electrostatic mechanism for substrate guidance down the aromatic gorge of acetylcholinesterase. Proc. Natl. Acad. Sci. U.S.A. 90, 5128–5132. https://doi.org/10.1073/pnas.90.11.5128.

Rosenberry, T.L., 1975. Acetylcholinesterase. Adv. Enzymol. 43, 103–218. https://doi.org/10.1002/9780470122884.ch3.

Rydzewski, J., Jakubowski, R., Nowak, W., Grubmüller, H., 2018. Kinetics of Huperzine A dissociation from acetylcholinesterase via multiple unbinding pathways. J. Chem. Theor. Comput. 14, 2843–2851. https://doi.org/10.1021/acs.jctc.8b00173.

Sanson, B., Colletier, J.P., Xu, Y., Lang, P.T., Jiang, H., Silman, I., Sussman, J.L., Weik, M., 2011. Backdoor opening mechanism in acetylcholinesterase based on X-ray crystallography and MD simulations. Protein Sci. 20, 1114–1118. https://doi.org/10.1002/pro.661.

Silman, I., Sussman, J.L., 2008. Acetylcholinesterase: how is structure related to function? Chem. Biol. Interact. 175, 3–10. https://doi.org/10.1016/j.cbi.2008.05.035.

Sussman, J.L., Harel, M., Frolow, F., Oefner, C., Goldman, A., Toker, L., Silman, I., 1991. Atomic structure of acetylcholinesterase from *Torpedo californica*: a prototypic acetylcholine-binding protein. Science 253, 872–879. https://doi.org/10.1126/science.1678899.

Touw, W.G., Joosten, R.P., Vriend, G., 2016. New biological insights from better structure models. J. Mol. Biol. 428, 1375–1393. https://doi.org/10.1016/j.jmb.2016.02.002.

Vigny, M., Bon, S., Massoulié, J., Leterrier, F., 1978. Active-site catalytic efficiency of acetylcholinesterase molecular forms in *Electrophorus, Torpedo*, rat and chicken. Eur. J. Biochem. 85, 317–323. https://doi.org/10.1111/j.1432-1033.1978.tb12241.x.

Wildman, S.A., Zheng, X., Sept, D., Auletta, J.T., Rosenberry, T.L., Marshall, G.R., 2011. Drug-like leads for steric discrimination between substrate and inhibitors of human acetylcholinesterase. Chem. Biol. Drug Des. 78, 495–504. https://doi.org/10.1111/j.1747-0285.2011.01157.x.

Winn, M.D., Ballard, C.C., Cowtan, K.D., Dodson, E.J., Emsley, P., Evans, P.R., Keegan, R.M., Krissinel, E.B., Leslie, A.G., McCoy, A., McNicholas, S.J., Murshudov, G.N., Pannu, N.S., Potterton, E.A., Powell, H.R., Read, R.J., Vagin, A., Wilson, K.S., 2011. Overview of the CCP4 suite and current developments. Acta Crystallogr. Sect. D Biol. Crystallogr. 67, 235–242. https://doi.org/10.1107/S0907444910045749.

Xu, Y., Cheng, S., Sussman, J.L., Silman, I., Jiang, H., 2017. Computational studies on acetylcholinesterases. Molecules 22, 1324. https://doi.org/10.3390/molecules22081324.

Xu, Y., Colletier, J.-P., Weik, M., Qin, G., Jiang, H., Silman, I., Sussman, J.L., 2010. Long route or shortcut? A molecular dynamics study of traffic of thiocholine within the active-site gorge of acetylcholinesterase. Biophys. J. 99, 4003–4011. https://doi.org/10.1016/j.bpj.2010.10.047.

Xu, Y., Shen, J., Luo, X., Silman, I., Sussman, J.L., Chen, K., Jiang, H., 2003. How does Huperzine A enter and leave the binding gorge of acetylcholinesterase? Steered molecular dynamics simulations. J. Am. Chem. Soc. 125, 11340–11349. https://doi.org/10.1021/ja029775t.

Zemella, A., Thoring, L., Hoffmeister, C., Kubick, S., 2015. Cell-Free protein synthesis: pros and cons of prokaryotic and eukaryotic systems. Chembiochem 16, 2420–2431. https://doi.org/10.1002/cbic.201500340.